Electrophoresis of a Membrane-Coated Cylindrical Particle Positioned Eccentrically along the Axis of a Narrow Cylindrical Pore

ARTICLE *in* THE JOURNAL OF PHYSICAL CHEMISTRY C · SEPTEMBER 2010

Impact Factor: 4.77 · DOI: 10.1021/jp105572a

Electrophoresis of a Membrane-Coated Cylindrical Particle Positioned Eccentrically along the Axis of a Narrow Cylindrical Pore

Li-Hsien Yeh and Jyh-Ping Hsu*

Department of Chemical Engineering, National Taiwan University, Taipei, Taiwan 10617

Shiojenn Tseng

Department of Mathematics, Tamkang University, Tamsui, Taipei, Taiwan 25137

Received: June 17, 2010; Revised Manuscript Received: August 18, 2010

Although theoretical analyses on electrophoresis are ample in the literature, most of them focused on the one- or two-dimensional problems for a simpler treatment; available results for the three-dimensional case, which may be closer to reality, are extremely limited. The electrophoresis of a soft, finite cylindrical particle positioned eccentrically along the axis of a narrow cylindrical pore is modeled in this study. The type of particle considered is capable of mimicking a wide class of nonrigid entities such as biocolloids and particles covered by an artificial polymer layer in practice. The electrophoretic behaviors of the particle under various conditions are simulated. We show that if the membrane layer of a particle is charged, then its electrophoretic behavior depends largely on its aspect ratio, eccentricity, and relative size, the thickness of double layer, and the thickness of the membrane layer, which might not be the case if that layer is uncharged. In addition, the electrophoretic mobility of a particle in the former may not increase with increasing thickness of the membrane layer, which has not been reported previously. The results gathered provide the theoretical basis for both the design of an electrophoresis apparatus and the interpretation of experimental data.

1. Introduction

The boundary effect on electrophoresis has been studied extensively in the past few decades. Because the presence of a nearby boundary is capable of influencing the neighboring concentration, electric, and flow fields of a particle, the associated forces acting on the particle are affected inevitably, so is its electrophoretic behavior. The influence of the boundary can be even more complicated if it is charged. The boundary effect is important, for example, in capillary electrophoresis where the linear size of the available space for electrophoresis is not very large compared with that of a particle. In the electrophoresis application such as electrodeposition, the boundary effect should not be ignored as a particle is sufficiently close to the electrode where it finally deposits. Modern technology often involves operations conducted in a micrometer- or submicrometer-scaled space. In this case, if the relevant phenomenon is driven by an applied electric file, then the methodologies used in the analysis of the boundary effect on electrophoresis can also be employed.

The boundary effect on electrophoresis has been studied by many researchers by considering various types of geometries such as a sphere in a spherical cavity[1−4] or normal to a plane,[5−7] and a sphere,[5,6,8−12] a cylinder,[13−17] an ellipsoid,[18] a toroid,[19] or two spheres[20] in a cylindrical pore. Liu et al.[14] considered the electrophoresis of a cylindrical particle in a long cylindrical pore. Under the conditions of long cylinder translating concentrically in a long tube, low surface potential, and thick double layer, an analytical result was derived, and numerical results were reported for an eccentrically positioned particle with a thin double layer. Assuming a thin double layer, Li and Daghighi[21] solved analytically the eccentric electrophoresis of a rectangular particle in a rectangular microchannel. Yariv and Brenner[8] investigated the electrophoresis of a sphere eccentrically positioned in a cylindrical pore for the case of thin double layers. The same problem was also analyzed numerically by Ye et al.[10] Hsu and Kuo[16] considered the electrophoresis of a rigid, finite cylinder positioned eccentrically along the axis of a long cylindrical pore for the case of arbitrary double layer thickness.

Conventional electrophoresis analyses are based mainly on rigid particles. Recent advances in various sciences and technologies urge relevant studies to focus on soft or fuzzy particles,[22−30] where a particle consists of a rigid core and a porous membrane or polymer layer. Biocolloids, for instance, are often simulated by a relatively rigid core enclosed by an ion-penetrable membrane layer. A colloidal dispersion stabilized by the introduction of surfactant is another typical example, where an original rigid particle is covered by adsorbed surfactant molecules forming a porous layer. Because the presence of a porous layer is capable of influencing both hydrodynamically and electrically the electrophoretic behavior of a soft particle,[31−36] the associated analysis is more complicated than that of the corresponding rigid particle. Assuming weak applied electric field and low surface potential, Ohshima conducted a series of studies on the electrophoresis of a soft particle.[37−42] Saville[43] and Hill et al.[44] analyzed the electrophoresis of an isolated soft spherical particle in an infinite electrolyte medium for the case where the effect of double-layer polarization (DLP) can be significant. Lee et al.[33] extended these analyses to take the effect of particle concentration into account. Several theoretical attempts have been made on the modeling of the electrophoresis of a soft particle under the conditions where the boundary effect can be significant. These include, for example, a sphere in an

* Corresponding author. Tel: 886-2-23637448. Fax: 886-2-23623040. E-mail: jphsu@ntu.edu.tw.

10.1021/jp105572a
Published on Web 09/03/2010

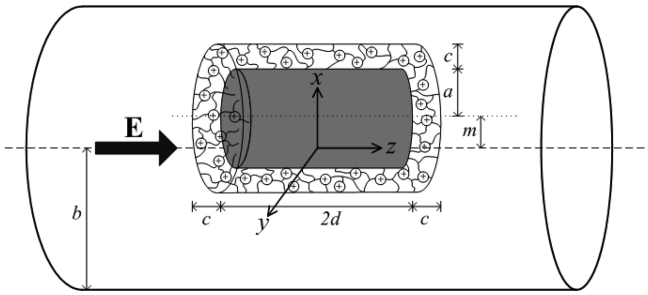

Figure 1. Electrophoresis of a soft cylinder comprising a rigid core of radius a and length $2d$ and an ion-penetrable membrane layer of thickness c parallel but eccentric to the axis of a long cylindrical pore of radius b. m is the distance between the axis of the particle and that of the pore; **E** is an applied uniform electric field parallel to the axis of the pore; and x, y, z are the Cartesian coordinates adopted with the origin at the center of the pore.

uncharged spherical cavity,[34] that normal to a large plane,[45] and that along the axis of a charged cylindrical pore.[35,36]

To simplify the analysis, previous electrophoresis studies are mainly of one- or two-dimensional nature, which can be unsatisfactory in practice because relevant phenomena are often three-dimensional. To examine the electrophoretic behavior of a particle under conditions closer to reality, we consider the electrophoresis of a soft cylindrical particle of finite length positioned eccentrically in a cylindrical pore, a three-dimensional problem. The pore considered simulates, for instance, the tube in capillary electrophoresis,[46,47] where its radius can be comparable to that of a particle. The type of particle assumed mimics, for instance, biocolloids such as protein and DNA. The influences of the size of the pore, the position of the particle, the thickness of electric double layer, and the physicochemical properties of the particle on its electrophoretic behavior are discussed in detail.

2. Theory

Let us consider the electrophoresis of a soft, finite cylindrical particle comprising a rigid core of radius a and length $2d$ and an ion-penetrable membrane layer of uniform thickness c positioned eccentrically along the axis of a narrow, nonconducting cylindrical pore of radius b illustrated in Figure 1. The pore is filled with an incompressible Newtonian fluid of constant physical properties. Let m be the distance between the axis of the particle and that of the pore and $P = [m/(b - a - c)] \times 100\%$ be the percentage of eccentricity. The Cartesian coordinates x, y, and z are adopted with the origin located at the center of the cylindrical pore, and a uniform electric field **E** of strength E is applied in the z-direction.

Under general conditions, the present problem is governed by a set of nonlinear, coupled partial differential equations, known as electrokinetic equations. These equations describe the spatial variations of the electrical potential, the concentration of ionic species, and the velocities of the fluid and the particle. Solving the electrokinetic equations is challenging, in general, and can be nontrivial even if they are solved numerically. Fortunately, simplifications that are realistic from the applications point of view can be made so that the difficulty of solving the general electrokinetic equations is alleviated. For instance, because the Debye length (or thickness of double layer) usually ranges from 1 nm to 1 μm, assuming the level of 250 mV for the upper limit of the surface potential would imply that the strength of the local electric field established by that potential ranges from 250 to 2.5×10^5 kV/m, which is much stronger than that of the applied electric field in practice. Therefore, for simplicity, we assume that E is much smaller than the strength of the local electric field established by the particle and/or the pore, and their surface potentials are sufficiently low.[5,27] Under these conditions, the electric potential ϕ can be expressed as a linear supposition of the equilibrium potential (the potential in the absence of **E**), ϕ_1, and a perturbed potential outside the particle arising from **E**, ϕ_2.[48] Then, it can be shown that, in terms of scaled symbols, these potentials can be described by[35,36]

$$\nabla^{*2}\phi_1^* = (\kappa a)^2\phi_1^* - h(\vec{r})Q^* \qquad h(\vec{r}) = 0, 1 \tag{1}$$

$$\nabla^{*2}\phi_2^* = 0 \tag{2}$$

Here, $\nabla^{*2} = a^2\nabla^2$ with ∇^2 being the Laplace operator; $Q^* = \rho_{fix}/(\varepsilon k_B T/ea^2)$, with ρ_{fix} and Q^* being the fixed charge density in the membrane layer of the particle and the corresponding scaled quantity, respectively; e, k_B, T, and ε are the elementary charge, Boltzmann constant, the absolute temperature, and the permittivity of the liquid phase, respectively; $\phi_k^* = \phi_k/\phi_{ref}$, $k = 1, 2$, is the scaled potentials with $\phi_{ref} = k_B T/e$ being a reference thermal electric potential; and $\kappa = [\Sigma_j n_{j0}(ez_j)^2/\varepsilon k_B T]^{1/2}$ is the reciprocal Debye length, with z_j and n_{j0} being the valence and the bulk number concentration of ionic species j, respectively. $h(\vec{r})$ is a unit step region index; $h(\vec{r}) = 0$ for the liquid phase outside the particle, and $h(\vec{r}) = 1$ for the region inside the membrane layer.

Under typical conditions, because the Reynolds number associated with electrophoresis is much smaller than unity the corresponding flow field is in the creeping flow regime. Following a similar treatment of Hsu et al.,[49] the flow field of the present problem can be described by the scaled equations[49,50]

$$-\nabla^* p^* + \nabla^{*2}\mathbf{u}^* + (\nabla^{*2}\phi_1^* + iQ^*)\nabla^*\phi_2^* - h(\vec{r})(\lambda a)^2(\mathbf{u}^* - \mathbf{U}/U_{ref}) = 0 \qquad h(\vec{r}) = 0, 1 \tag{3}$$

$$\nabla^* \cdot \mathbf{u}^* = 0 \tag{4}$$

In these expressions, $\mathbf{u}^* = \mathbf{u}/U_{ref}$ with $U_{ref} = \varepsilon(\phi_{ref})^2/\eta a$ being a reference velocity, where **u** and η are the velocity and the viscosity of the liquid phase, respectively. $(\lambda a) = (\gamma a^2/\eta)^{1/2}$ is the scaled friction coefficient of the membrane layer, with γ being the corresponding frictional coefficient. $(\lambda a)^2(\mathbf{u}^* - \mathbf{U}/U_{ref})$ represents the scaled hydrodynamic drag acting on the membrane layer by the interstitial fluid with **U** being the particle velocity. Here, λ^{-1} is the softness parameter of the membrane layer,[29] which also represents a shielding length characterizing the extent of flow penetration into that layer.[50] $p^* = p/p_{ref}$, where p, p^*, and $p_{ref} = \varepsilon(\phi_{ref})^2/a^2$ are the pressure, the scaled pressure, and a reference pressure, respectively.

We assume that the surface of the rigid core of the particle is remained at a constant potential ζ_p, and it is nonconductive, impermeable to ionic species, and nonslip. These yield the following boundary conditions:

$$\phi_1^* = \zeta_p/\phi_{ref} \qquad \text{on the rigid core surface} \tag{5}$$

$$\mathbf{n}\cdot\nabla^*\phi_2^* = 0 \qquad \text{on the rigid core surface} \tag{6}$$

$$\mathbf{u}^* = \mathbf{U}/U_{\text{ref}} \qquad \text{on the rigid core surface} \tag{7}$$

Here, $\nabla^* = a\nabla$, with ∇ being the gradient operator; $\mathbf{n}$ is the unit normal vector directed into the liquid phase. Equation 6 implies that the application of $\mathbf{E}$ will not induce any charge on the surface of the rigid core of the particle.

Let Ω_i, Ω_o, and Ω_b be the inlet surface, the outlet surface, and the inner surface of the cylindrical pore, respectively. Suppose that Ω_b is uncharged, nonconductive, and nonslip. Then the following boundary conditions apply:

$$\phi_1^* = \zeta_b/\phi_{\text{ref}} = 0 \qquad \text{on } \Omega_b \tag{8}$$

$$\phi_1^* = 0 \qquad \text{on } \Omega_i \text{ and } \Omega_o \tag{9}$$

$$\mathbf{n}\cdot\nabla^*\phi_2^* = 0 \qquad \text{on } \Omega_b \tag{10}$$

$$\nabla^*\phi_2^* = -E^*\mathbf{e}_z \qquad \text{on } \Omega_i \text{ and } \Omega_o \tag{11}$$

$$\mathbf{u}^* = 0 \qquad \text{on } \Omega_b \tag{12}$$

$$\mathbf{u}^* = 0 \qquad \text{on } \Omega_i \text{ and } \Omega_o \tag{13}$$

Here, $E^* = E/[(\phi_{\text{ref}})/a]$, with ζ_b and $\mathbf{e}_z$ being the surface potential on Ω_b and the unit vector in the z-direction, respectively.

For simplicity, we assume that the permittivity ε and the viscosity η of the liquid phase inside the membrane layer are the same as those outside it. In addition, the fixed charge in the membrane is uniformly distributed; that is, ρ_{fix} is position-independent.[27] Under these conditions, the following continuous boundary conditions are applicable on the particle surface (i.e., the interface between the membrane layer and the external fluid), Ω_p:[27,35,36]

$$\phi_1^*|_{\Omega_p^-} = \phi_1^*|_{\Omega_p^+} \qquad \text{and} \qquad \mathbf{n}\cdot\nabla^*\phi_1^*|_{\Omega_p^-} = \mathbf{n}\cdot\nabla^*\phi_1^*|_{\Omega_p^+} \tag{14}$$

$$\phi_2^*|_{\Omega_p^-} = \phi_2^*|_{\Omega_p^+} \qquad \text{and} \qquad \mathbf{n}\cdot\nabla^*\phi_2^*|_{\Omega_p^-} = \mathbf{n}\cdot\nabla^*\phi_2^*|_{\Omega_p^+} \tag{15}$$

$$\mathbf{u}^*|_{\Omega_p^-} = \mathbf{u}^*|_{\Omega_p^+}, \qquad \mathbf{n}\cdot\mathbf{u}^*|_{\Omega_p^-} = \mathbf{n}\cdot\mathbf{u}^*|_{\Omega_p^+}, \quad \text{and} \quad \mathbf{n}\times\mathbf{u}^*|_{\Omega_p^-} = \mathbf{n}\times\mathbf{u}^*|_{\Omega_p^+} \tag{16}$$

$$\mathbf{n}\cdot(\boldsymbol{\sigma}^{\mathbf{H}^*}\cdot\mathbf{n})|_{\Omega_p^-} = \mathbf{n}\cdot(\boldsymbol{\sigma}^{\mathbf{H}^*}\cdot\mathbf{n})|_{\Omega_p^+} \qquad \text{and} \qquad \mathbf{n}\times(\boldsymbol{\sigma}^{\mathbf{H}^*}\cdot\mathbf{n})|_{\Omega_p^-} = \mathbf{n}\times(\boldsymbol{\sigma}^{\mathbf{H}^*}\cdot\mathbf{n})|_{\Omega_p^+} \tag{17}$$

Here, $\boldsymbol{\sigma}^{\mathbf{H}^*} = \boldsymbol{\sigma}^{\mathbf{H}}/[\varepsilon(\phi_{\text{ref}})^2/a^2]$ is the scaled hydrodynamic stress tensor with $\boldsymbol{\sigma}^{\mathbf{H}} = -p\mathbf{I} + 2\eta\boldsymbol{\Delta}$ being the corresponding hydrodynamic stress tensor; $\mathbf{I}$ and $\boldsymbol{\Delta} = [\nabla\mathbf{u} + (\nabla\mathbf{u})^{\mathbf{T}}]/2$ are the unit tensor and the rate of deformation tensor, respectively; the superscript $\mathbf{T}$ denotes the matrix transpose. Note that, due to the nature of the particle−external fluid interface, specifying a continuous boundary condition for ϕ_1^*, ϕ_2^*, $\mathbf{u}^*$, and p^* is unnecessary because it will be satisfied automatically in the solution produced.

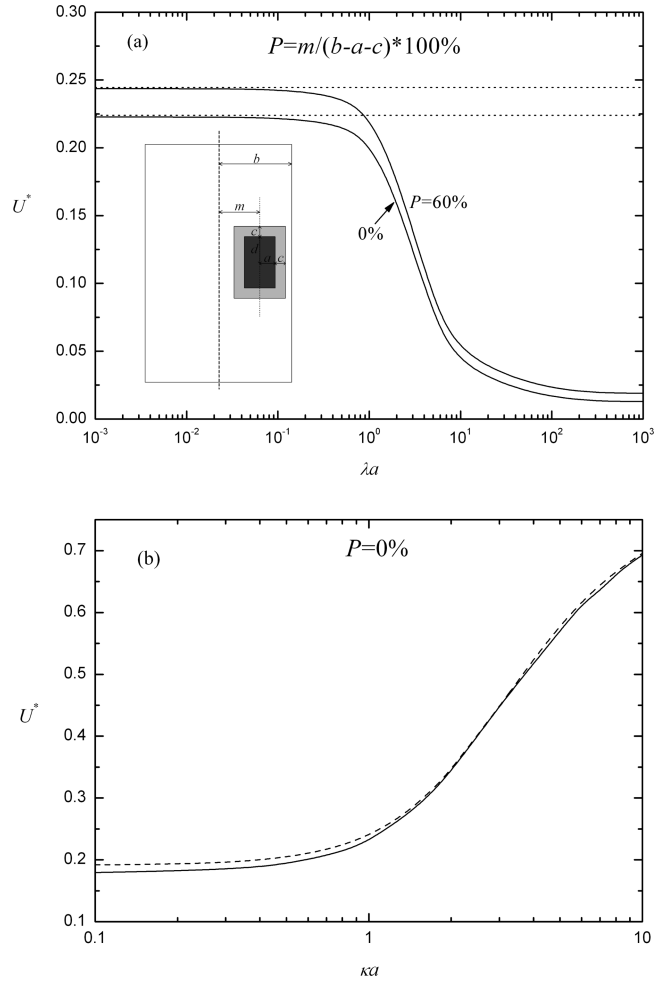

Figure 2. Variation of the scaled electrophoretic mobility U^* of a cylindrical soft particle as a function of λa for two levels of P at $d/a = 1$ and $\kappa a = 1$ (a), and as a function of κa at $P = 0\%$, $d/a = 10$, and $\lambda a = 0.01$ (b) for the case where the rigid core of the particle is positively charged and the pore uncharged at $b/a = 2$, $c/a = 0.5$, and $Q^* = 0$. Key: solid curves, numerical results; dotted curves, numerical results of Hsu and Kuo;[16] dashed curves, analytical results of Liu et al.[14] at $L_T/L_C = 100$ with L_T and L_C being the length of the pore and that of the particle, respectively. Other parameters used are $\zeta_p^* = \zeta_p/(k_BT/e) = 1$ and $\zeta_b^* = \zeta_b/(k_BT/e) = 0$.

In the present problem, the forces acting on the particle include mainly the electrical force and the hydrodynamic force. The geometry considered suggests that only the z-component of these forces, F_E and F_D, respectively, need be considered. F_E and F_D can be obtained by integrating the Maxwell stress tensor[49,51] and the hydrodynamic stress tensor,[49,52] respectively, over Ω_p. It can be shown that[36,49,52]

$$\begin{aligned} F_E^* &= \int_{\Omega_p^*}\int (\boldsymbol{\sigma}^{\mathbf{E}^*}\cdot\mathbf{n})\cdot\mathbf{e}_z \, d\Omega_p^* \\ &= \int_{\Omega_p^*}\int \left[\frac{\partial\phi_1^*}{\partial n}\frac{\partial\phi_2^*}{\partial z^*} + \frac{\partial\phi_2^*}{\partial n}\frac{\partial\phi_1^*}{\partial z^*}\right] - \\ &\qquad \left[\frac{\partial\phi_1^*}{\partial n}\frac{\partial\phi_2^*}{\partial n} + \frac{\partial\phi_1^*}{\partial t}\frac{\partial\phi_2^*}{\partial t}\right] n_z \, d\Omega_p^* \end{aligned} \tag{18}$$

and

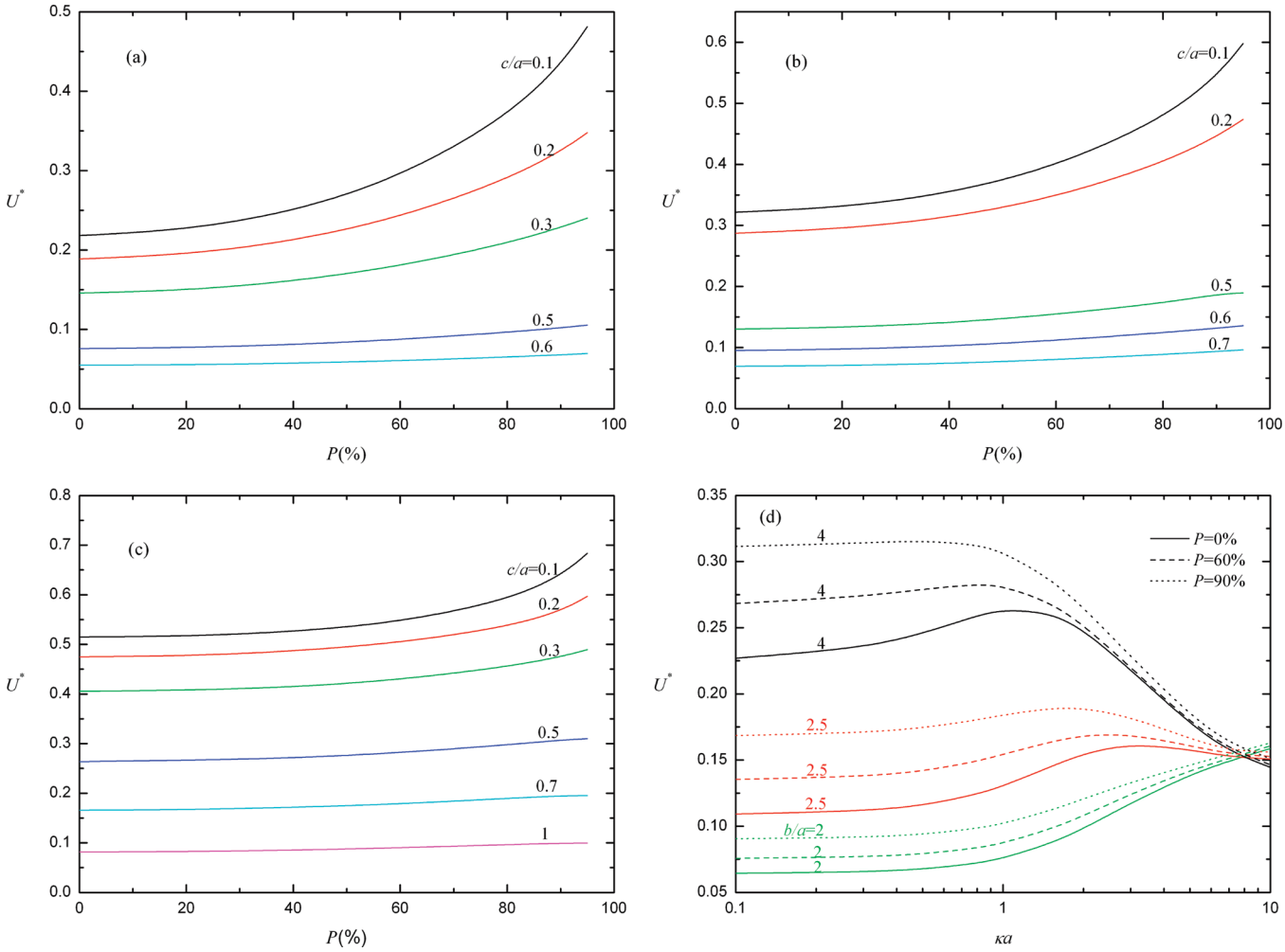

Figure 3. Variations of the scaled electrophoretic mobility U^* as a function of P for various combinations of (b/a) and (c/a) at $\kappa a = 1$ (a)−(c) and as a function of κa for various combinations of (b/a) and P at $c/a = 0.5$ (d) for the case where $Q^* = 0$, $\lambda a = 5$, and $d/a = 1$: (a) $b/a = 2$; (b) $b/a = 2.5$; (c) $b/a = 4$.

$$F_D^* = \int_{\Omega_p^*} \int (\boldsymbol{\sigma}^{H*} \cdot \mathbf{n}) \cdot \mathbf{e}_z \, d\Omega_p^* \tag{19}$$

Here, $F_E^* = F_E/\varepsilon(\phi_{ref})^2$ and $F_D^* = F_D/\varepsilon(\phi_{ref})^2$ are the scaled electrical force and the scaled hydrodynamic force, respectively; $\boldsymbol{\sigma}^{E*} = \boldsymbol{\sigma}^E/[\varepsilon(\phi_{ref})^2/a^2]$ is the scaled form of Maxwell stress tensor, with $\boldsymbol{\sigma}^E = \varepsilon \mathbf{E}\mathbf{E} - (1/2)\varepsilon E^2 \mathbf{I}$ being the corresponding Maxwell stress tensor, where $E^2 = \mathbf{E} \cdot \mathbf{E}$. $z^* = z/a$, and $\Omega_p^* = \Omega_p/a^2$ is the scaled particle surface area; n_z, n, and t are the magnitude of the z-component of the unit normal vector $\mathbf{n}$, that of $\mathbf{n}$, and that of the unit tangential vector $\mathbf{t}$, respectively.

If we assume that the system is at a pseudosteady state, that is, if the sum of the relevant forces acting on the particle vanishes, then

$$F_E^* + F_D^* = 0 \tag{20}$$

To avoid a tedious trial-and-error procedure in the resolution of the governing equations subject to the specified boundary conditions, the approach similar to that proposed by O'Brien and White[53] is adopted. In this approach, the original electrophoresis problem is partitioned into two subproblems: (1) the particle moves with a constant velocity U in the absence of $\mathbf{E}$, and (2) $\mathbf{E}$ is applied but the particle is held fixed. In subsequent discussions, symbols with subscript i denote the properties in subproblem i, $i = 1, 2$. In the first subproblem, the particle experiences a scaled conventional hydrodynamic force $F_{D,1}^* = -[U/\varepsilon(\phi_{ref})^2]D$, where the drag coefficient D is positive and its value depends only on the geometry of the system considered and the frictional coefficient of the membrane layer but is independent of the thickness of the double layer and the fixed charge density in the membrane layer. In the second subproblem, the particle experiences both an electrical force and a drag force. Let F_E^* and $F_{D,2}^*$ be the scaled forms of these forces, respectively. The latter is the scaled electroosmotic retardation force[20] coming from the motion of the mobile ions in the electric double layer due to the application of $\mathbf{E}$. Note that $F_{D,2}^*$ is a function of P, ka, (d/a), (c/a), λa, and Q^*; F_E^* is a function of P, ka, (d/a), (c/a), and Q^* but is independent of λa.[15,16] Substituting $F_D^* = F_{D,1}^* + F_{D,2}^*$ with $F_{D,1}^* = -[U/\varepsilon(\phi_{ref})^2]D$ into eq 20 and letting $U^* = U/U_E$ be the scaled electrophoretic mobility of the particle, we obtain

$$U^* = \frac{F_E^* + F_{D,2}^*}{D^*} \tag{21}$$

where $D^* = D/[\varepsilon(\phi_{ref})^2/U_{ref}]$ is the scaled drag coefficient resulting from the hydrodynamic drag.

3. Results and Discussion

The governing equations and the associated boundary conditions are solved numerically by FlexPDE (PDE Solutions, Spokane Valley, WA), which is based on a finite-element method. Grid independence is checked throughout numerical calculations. For the present three-dimensional problem, using a total of ca. 36 000 and 16 000 nodes is sufficient for the resolution of the electric and the flow fields, respectively. The end effect of the cylindrical pore can be neglected if its length exceeds ca. 10 times the particle length.[15,16] For illustration, we assume that $\zeta_p^* = \zeta_p/(k_BT/e) = 1$ and $\zeta_b^* = \zeta_b/(k_BT/e) = 0$. The latter applies, for example, to the case of a fused-silica pore coated with a hydrophobic thin film such as a cross-linked polyacrylamide or poly(vinyl alcohol).[54]

The applicability of the numerical procedure adopted is first examined by applying it to the case of the electrophoresis of a rigid cylinder along the axis of a long cylindrical pore under the conditions of weak applied electric field and low surface potential. This problem was solved previously by Hsu and Kuo[16] and Liu et al.[14] To simulate their rigid particles, the membrane layer of the present soft particle is assumed to be uncharged and is assigned a small λa. Figure 2 shows the variations of the scaled electrophoretic mobility of a particle U^* under various conditions; both the results in the literature[14,16] and the corresponding results based on the present approach are presented. Note that if $\lambda a \rightarrow 0$, then the membrane layer of the present soft particle becomes frictionless to the fluid flow, and it is equivalent to a rigid particle of smaller radius,[33,37,42] which is justified by Figure 2. Figure 2b indicates that the difference between the present results and that of Liu et al.[14] is more appreciable as smaller values of κa, which is consistent with the previous results.[15,17] This is because, if the double layer is sufficiently thick, then the end effect of the pore becomes significant. In general, Figure 2 reveals that the performance of the present numerical procedure is satisfactory.

In subsequent discussions, the electrophoretic behaviors of a particle under various conditions are simulated through varying the parameters key to the present problem. These include the thickness of the double layer, the size of the pore, and the position and physicochemical properties of the particle. Typically, the linear size of a particle ranges from 10^{-3} to 10 μm and that of a pore from 10^{-2} to 100 μm. The magnitude of the softness parameter λ^{-1} ranges from 0.1 to 10 nm.[29,55−60] The ranges of the relevant parameters considered later are based on these values. For illustration, two representative cases are examined, namely, the membrane layer is uncharged ($Q^* = 0$) and it is positively charged with $Q^* = 10$. In addition, we assume that the thickness of the membrane layer does not exceed one-tenth of the radius of the rigid core, that is, $c/a \leq 1$.

3.1. Uncharged Membrane ($Q^* = 0$). In this case, the membrane layer is free of fixed charge. Figure 3 shows the variations of the scaled electrophoretic mobility of a particle U^* at various combinations of the percentage eccentricity P, the scaled thickness of membrane layer (c/a), the relative size of the pore to that of the particle (b/a), and the thickness of double layer κa. The corresponding variations of the scaled drag coefficient D^* and the scaled forces, F_E^*, $F_{D,2}^*$, and F_2^* ($= F_E^* + F_{D,2}^*$), are illustrated in Figure 4. Because a is fixed, the variation of κa arises from that of the concentration of electrolytes. Figure 3a−c indicates that for fixed values of (b/a) and P, U^* decreases with increasing (c/a). This is because the membrane layer is free of fixed charge, and therefore, the thicker it is, the greater the friction force for the fluid flow inside and the greater the hydrodynamic drag acting on the particle. Figure 3 also suggests

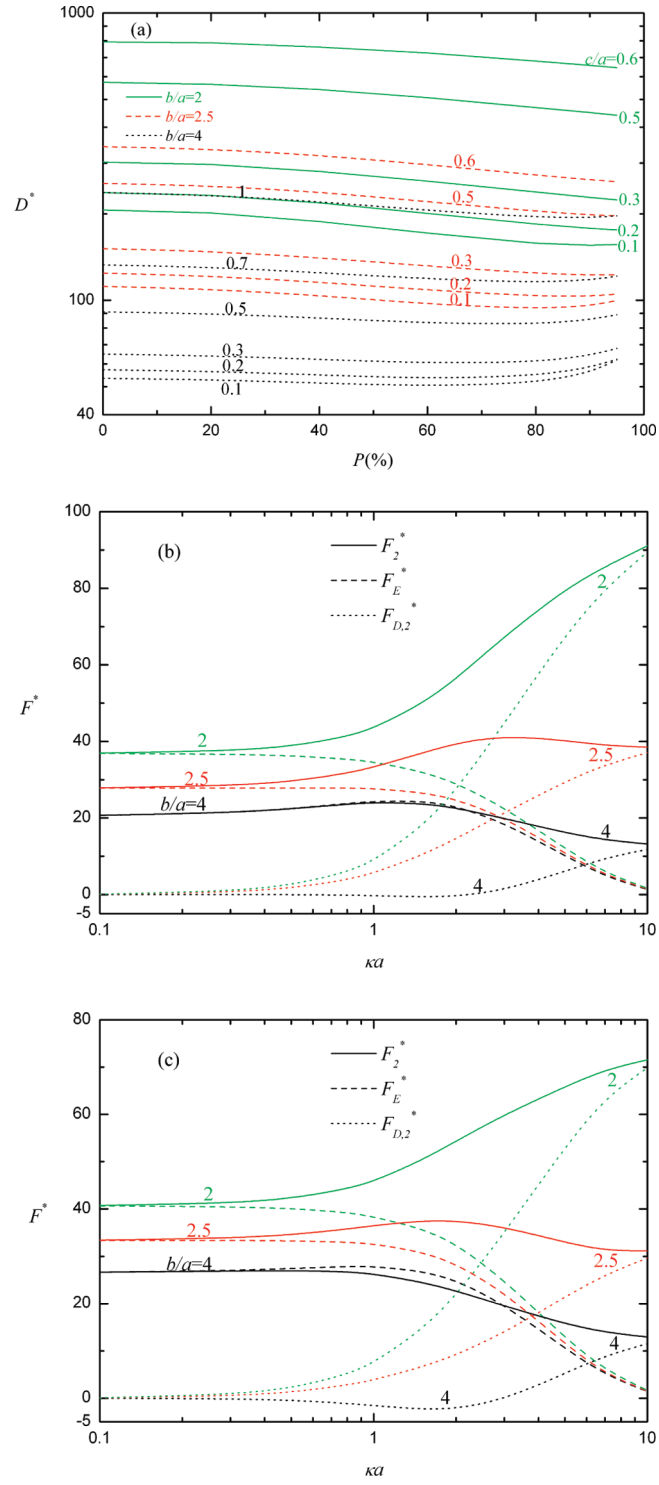

Figure 4. Variations of the scaled drag coefficient D^* for the case of Figure 3a−c (a), that of the scaled forces, F_E^*, $F_{D,2}^*$, and F_2^* for the case of Figure 3d at $P = 0\%$ (b), and that at $P = 90\%$ (c).

that, regardless of the levels of (c/a) and (b/a), U^* increases with increasing P; that is, the closer the particle to the boundary, the larger its scaled mobility. Similar behavior was also observed in the electrophoresis of a rigid cylinder positioned eccentrically along the axis of a cylindrical pore[14,16] and that of a rigid sphere parallel to a nonconducting planar wall.[6,61] That behavior of U^* can be explained by the results shown in Figure 4. As seen in this figure, if κa is sufficiently large, then because the double layer is enclosed by the membrane layer, the effective flow region inside the latter is large. In this case, since the scaled

electrical force F_E^* is relatively small, U^* is dominated either by D^* if it decreases with increasing P, or by the scaled electroosmotic retardation force $F_{D,2}^*$, if it increases with increasing P. On the other hand, if κa is small and/or (c/a) is sufficiently small, then U^* becomes dominated by F_E^*. This is because, as a charged particle approaches a neutral pore, the contours of the electrical potential (or double layer) surrounding the former is distorted and its surface charge density increases according. In addition, the local electric field between the particle and the pore is squeezed by the later.[15,16] Both of these two effects lead to an increase in F_E^*, and therefore, in U^*. As pointed out by Hsu and Kuo,[16] the influence of P on U^* is enhanced by an increase in (b/a) large, which is justified in Figure 3. As seen in Figure 3c, U^* is insensitive to the variation of P except that when (c/a) is sufficiently small, implying that if (c/a) is large, then the influence of the boundary on the mobility of the particle is unimportant. Figure 3d reveals that if κa is small, then regardless of the level of P, U^* increases with increasing (b/a); however, if κa is sufficiently large, the reverse trend is observed. The former was also observed in similar electrophoresis problems,[34−36] and can be explained by that the larger the (b/a) the less significant the boundary effect is. The later has not been reported previously. This is because if κa is small, then the rate of decrease in D^* as (b/a) increases is slower than that in F_2^*, but that trend becomes reversed if κa is sufficiently large. Note that D^* increases with decreasing (b/a) but is independent of κa,[2,15,20] implying that for the case where the membrane layer of the particle is uncharged, if the double layer is thick, its electrophoretic behavior is dominated by the hydrodynamic drag (D^*) as (b/a) varies. On the other hand, if the double layer is sufficiently thin, then that behavior is dominated by the driving forces associated with the electrical factor (F_E^* and $F_{D,2}^*$). As seen in Figure 3d, the qualitative behavior of U^* as κa varies depends largely upon (b/a) and/or P. For example, regardless of the level of P, if (b/a) is sufficiently small, then U^* increases monotonically with increasing κa. However, if (b/a) is large, then U^* may have a local maximum as κa varies. These behaviors are similar to those in the case of a membrane-coated sphere at the center of a spherical cavity[34] and along the axis of a cylindrical pore,[35] where the membrane layer is positively charged. The presence of a local maximum in U^* as κa varies was observed experimentally in the electrophoresis of shewanella bacteria (BrY1),[62] where its polyelectrolyte layer is negatively charged. The behaviors of U^* seen in Figure 3d are similar to those of F_2^* in Figure 4b,c, implying that the former comes from the competition of the driving forces F_E^* and $F_{D,2}^*$ as P, (b/a), and κa vary. If (b/a) is small (boundary effect is significant), then the behavior of U^* is dominated by $F_{D,2}^*$; otherwise, it is dominated by F_E^*. If (b/a) takes a medium large value (2.5), the behavior of U^* is dominated by $F_{D,2}^*$ when κa is small (thick double layer), and by F_E^* when it is large. Figure 4b,c reveals that at $c/a = 0.5$, if (b/a) is not large and/or P is sufficiently large, F_E^* decreases with increasing κa; if (b/a) is sufficiently large and/or P is sufficiently small, then F_E^* has a local maximum as κa varies. The former is because the larger the κa, the thinner the double layer and the greater the amount of counterions confined in the interior of the membrane layer, which has the effect of reducing the electrical force. In this case, if κa is small, then F_E^* decreases only slightly with increasing κa but becomes appreciable if κa is large. A larger κa also implies a greater gradient of the electrical potential on the surface of the rigid core of the particle, a higher surface charge density, and a greater electrical force. Note that this effect is alleviated if the

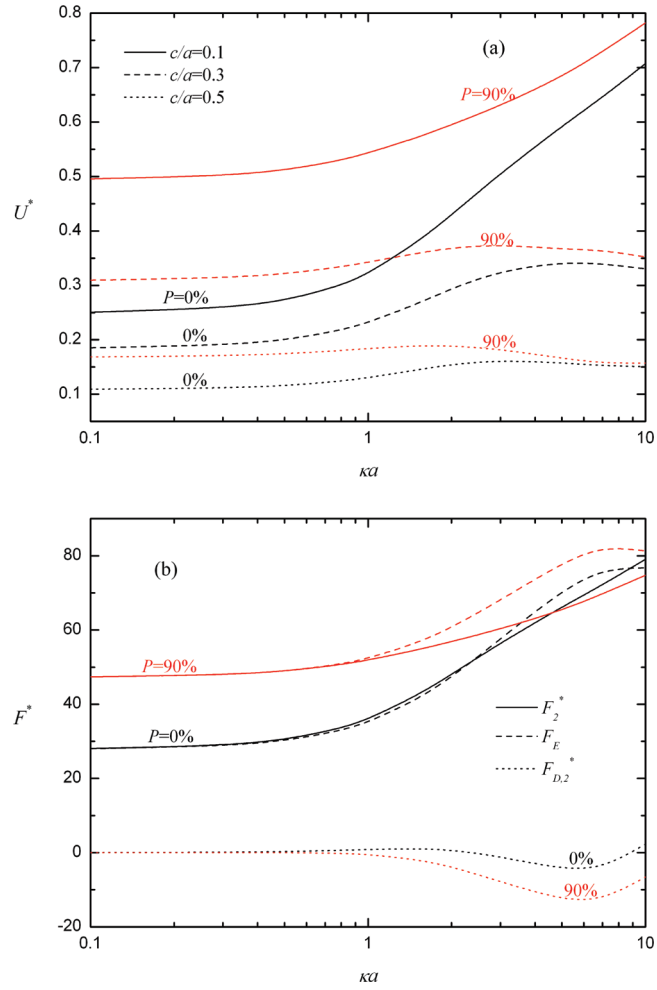

Figure 5. Variations of the scaled electrophoretic mobility U^* as a function of κa for various combinations of (c/a) and P at $b/a = 2.5$ and $d/a = 1$ for the case where $Q^* = 0$ and $\lambda a = 5$ (a) and that of the scaled forces, F_E^*, $F_{D,2}^*$, and F_2^* for the case of Figure 5a at $c/a = 0.1$ (b).

overlapping between the double layer of the particle with the boundary is significant,[15] which occurs when (b/a) is small and/or P is large.[2] If that effect dominates, then the larger the κa, the greater the F_E^*. Figure 4b,c also indicates that whereas F_E^* is always positive, $F_{D,2}^*$ can be negative or positive. This is because the hydrodynamic stress tensor comprises both a pressure component and a viscous component,[49,52] that is, $F_{D,2}^*$ can be expressed as[2,20]

$$F_{D,2}^* = \frac{F_{D,2}}{\varepsilon(\phi_{ref})^2} = F_{D,2(v)}^* + F_{D,2(p)}^* \qquad (22)$$

$F_{D,2(v)}^* = F_{D,2(v)}/\varepsilon(\phi_{ref})^2$ is the viscous component of $F_{D,2}^*$, and its magnitude depends upon the rate of strain of the fluid moving across the particle surface. $F_{D,2(p)}^* = F_{D,2(p)}/\varepsilon(\phi_{ref})^2$ is the pressure component of $F_{D,2}^*$, and its magnitude depends upon the strength of the pressure field. For the present case, $F_{D,2(p)}^*$ is always positive, but $F_{D,2(v)}^*$ can be positive or negative, depending on the level of (b/a). If (b/a) is sufficiently large and κa is small, because the rate of strain across the particle surface is negative, $F_{D,2}^*$ is dominated by a negative $F_{D,2(v)}^*$. On the other hand, if (b/a) is sufficiently small and/or κa is large, then the rate of strain across the particle surface becomes positive and increases with increasing κa, so are $F_{D,2(v)}^*$ and $F_{D,2}^*$. It is interesting to

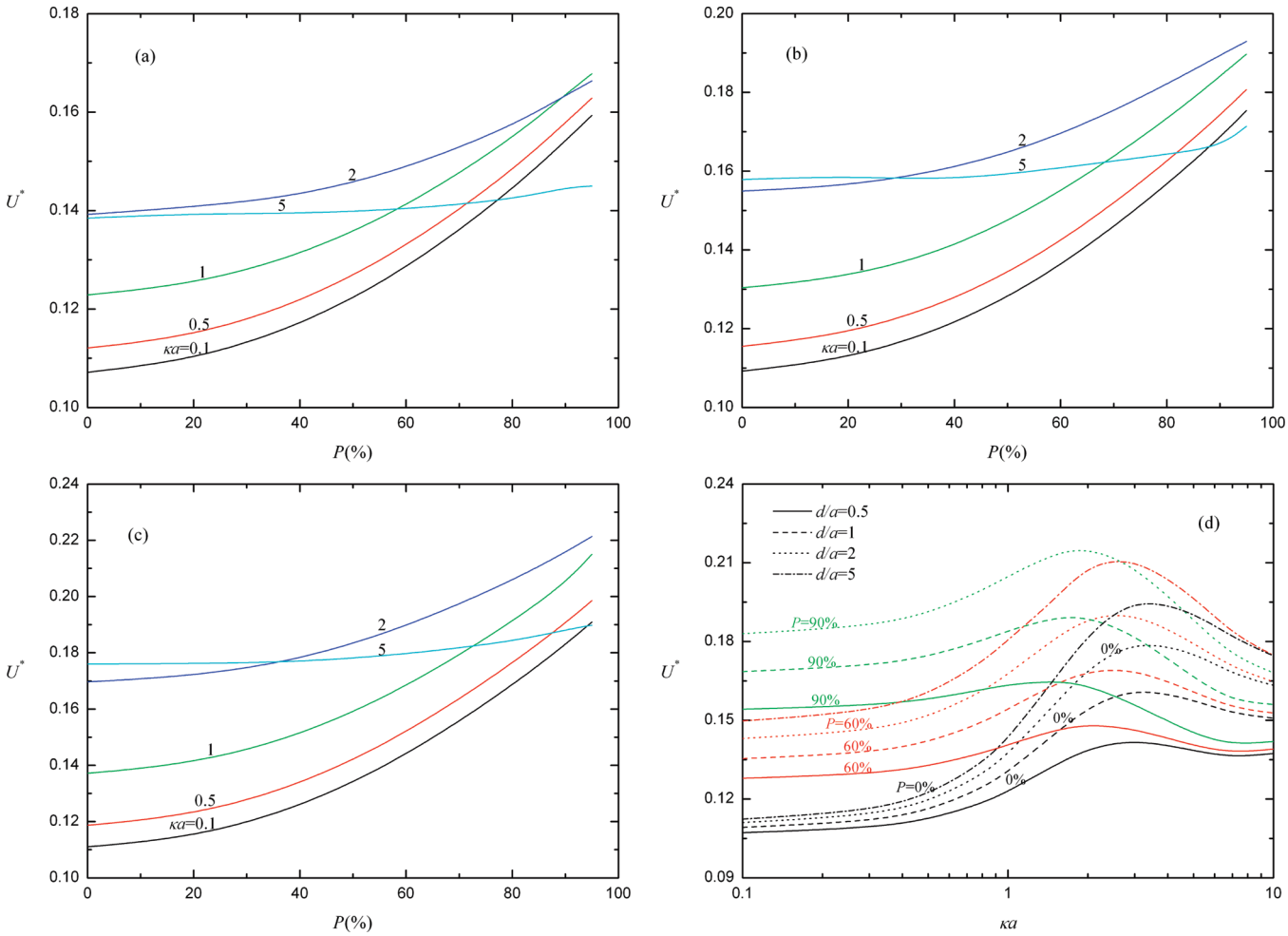

Figure 6. Variations of the scaled electrophoretic mobility U^* as a function of P for various combinations of (d/a) and κa at $b/a = 2.5$ and $c/a = 0.5$ (a)−(c) and as a function of κa for various combinations of (d/a) and P at $b/a = 2.5$ and $c/a = 0.5$ (d) for the case where $Q^* = 0$ and $\lambda a = 5$: (a) $d/a = 0.5$; (b) $d/a = 1$; (c) $d/a = 2$.

note that the value of κa at which U^* has the local maximum increases with increasing (b/a) or P. This is because, as κa increases, F_E^* decreases more rapidly if (b/a) or P is larger, as is shown in Figure 4b,c. As seen in Figure 4a, D^* increases with increasing (c/a) and/or decreasing (b/a). This is because the thicker the membrane layer and/or the more significant the boundary effect, the greater the hydrodynamic drag force. Figure 4a also shows that the relationship between D^* and P depends upon the levels of (b/a) and (c/a). For example, if (b/a) is sufficiently small and (c/a) is sufficiently large, then D^* decreases monotonically with increasing P; if (b/a) is large and (c/a) is small, then D^* might have a local minimum as P varies. These behaviors are similar to those observed in the case of a rigid cylinder positioned eccentrically in a cylindrical pore[16] and can be explained by the same reasoning.

Figure 5 shows the variations of the scaled electrophoretic mobility of a particle U^* as a function of κa at various combinations of (c/a) and P, and the corresponding variations of the scaled forces F_E^*, $F_{D,2}^*$, and F_2^* at $c/a = 0.1$. It is interesting to note that the qualitative behavior of U^* as κa varies depends upon the level of (c/a). If (c/a) is small, the influence of the membrane layer of a soft particle on its electrophoretic behavior is insignificant. In this case, U^* is seen to increase with increasing κa, which is similar to the behavior of the U^* for a rigid cylinder.[14−17] However, if (c/a) is large, that influence becomes significant. In this case U^* has a local maximum as κa varies, which is consistent with the result shown in Figure 3d. The result that U^* increases with increasing κa arises mainly from the increase in the scaled net driving force F_2^*, as is illustrated in Figure 5b, which is also observed in the case of a rigid cylinder.[15,16] Figure 5b indicates that if κa is small, F_E^* increases with increasing κa, but that trend is reversed if κa is sufficiently large. The former is expected, and the later can be explained by the same reasoning as that employed in the discussion of Figure 4b,c. Note that in the present case $(c/a = 0.1)$, although $F_{D,2(p)}^*$ is always positive, $F_{D,2(v)}^*$ is negative at small κa and has a negative local minimum as κa varies. However, if P is small, then $F_{D,2(v)}^*$ might change its sign from negative to positive at a sufficiently large κa, so is $F_{D,2}^*$ .This is why $F_{D,2}^*$ shows a negative local minimum in Figure 5b as κa varies.

The variations of U^* at various combinations of P, κa, and (d/a) are presented in Figure 6, and the corresponding variations of the scaled forces F_E^*, $F_{D,2}^*$, and F_2^* for the case of Figure 6d at $P = 0\%$ are illustrated in Figure 7. As seen in Figure 6, regardless of the level of κa and (d/a), U^* increases with increasing P, which is consistent with the result shown in Figure 3 and can be explained by similar reasoning. As seen in Figure 6d, where $b/a = 2.5$, U^* has a local maximum as κa varies, which is consistent with the result shown in Figure 3d. Note that if $d/a = 0.5$, U^* also has a local minimum at a large value of κa. Again, these phenomena arise from the competition between F_E^* and $F_{D,2}^*$. As expected, the qualitative behavior of U^* as κa varies is similar to that of F_2^* shown in Figure 7

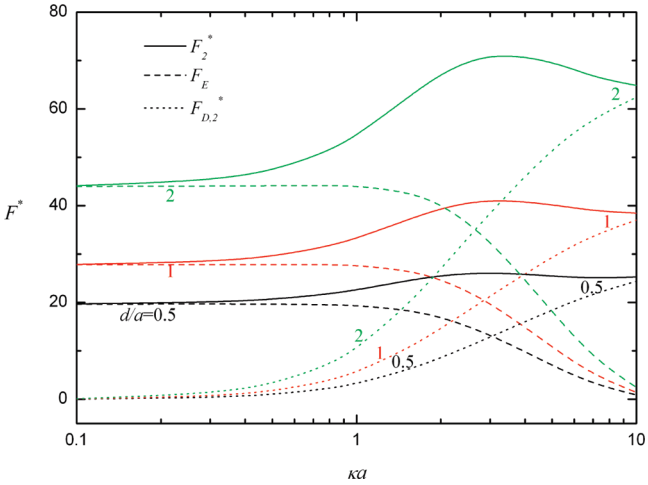

Figure 7. Variations of the scaled forces, F_E^*, $F_{D,2}^*$, and F_2^* for the case of Figure 6d at $P = 0\%$.

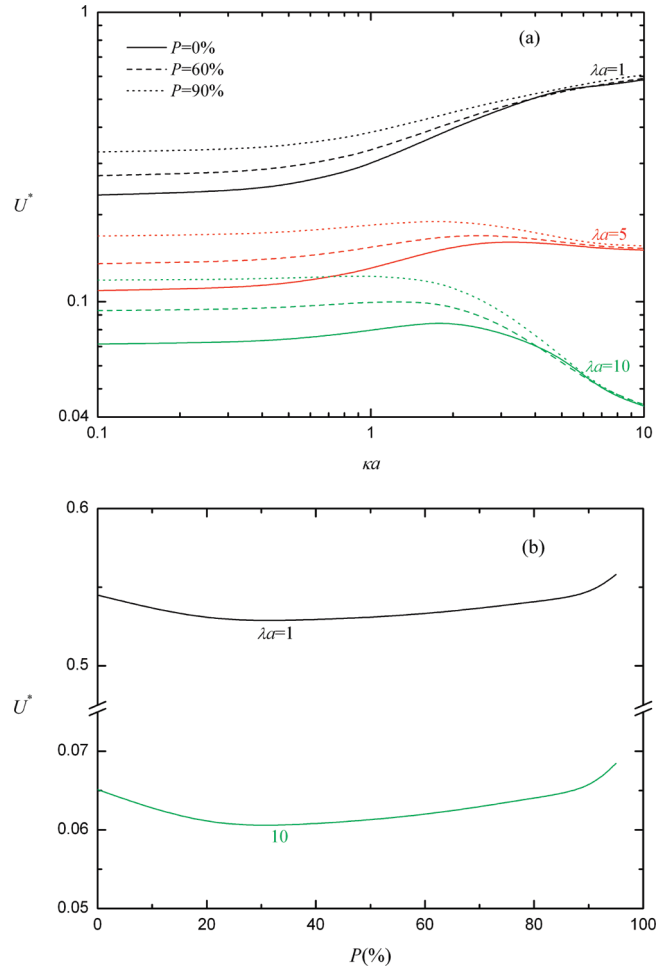

Figure 8. Variations of the scaled electrophoretic mobility U^* as a function of κa for various combinations of λa and P at $b/a = 2.5$, $c/a = 0.5$, $d/a = 1$, and $Q^* = 0$ (a) and as a function of P for two levels of λa at $\kappa a = 5$ for the case of Figure 8a (b).

because D^* is independent of κa in the present case.[15,20,35] In Figure 7 ($d/a = 0.5$), if κa is either sufficiently small or sufficiently large, then $F_{D,2}^*$ dominates, and if it takes a medium large value, F_E^* dominates. Note that, regardless of the levels of κa and P, U^* always increases with increasing (d/a). This is because as (d/a) increases, the rate of increase in the scaled net driving force F_2^* is always faster than that in D^*. In the present case, the behaviors of U^* at different levels of (d/a) are quite different from those in the case of a rigid cylinder,[15,17,63] where U^* decreases (increases) with increasing (d/a) when κa is small (large). Again, this implies that the electrophoretic behavior of a particle is influenced both qualitatively and quantitatively by its membrane layer if it is sufficiently thick.

The influence of the friction coefficient of the membrane layer of a particle, measured by λa, on its electrophoretic behavior is illustrated in Figure 8. This figure indicates that, regardless of the values of κa and P, U^* decreases with increasing λa, which is consistent with the results of similar electrophoresis problems.[33−36,41,43] This is because the larger the λa the greater the friction force arising from the presence of the membrane layer. Figure 8a shows that the relationship between U^* and κa depends largely on the levels of λa: if λa is small, U^* decreases with increasing κa, and if λa is large, then U^* has a local maximum as κa varies. These behaviors are consistent with those observed by Hsu et al.[35] for the case of a soft sphere in a cylindrical pore and can be explained by the same reasoning.[35] Note that if κa is sufficiently large, then for both the case where λa is sufficiently small and where it is sufficiently large, U^* has a local minimum as P varies, as is illustrated in Figure 8b. This local minimum disappears, however, if κa is too large. The presence of the local minimum in U^* is also observed by Ye et al.[10] for the eccentric electrophoresis of a rigid sphere in a cylindrical microchannel and by Hsu and Kuo[16] for the eccentric electrophoresis of a rigid cylinder along the axis of a cylindrical pore, which justify the results shown in Figure 8. Again, the presence of the local minimum in U^* as P varies can be explained by the behaviors of F_E^*, $F_{D,2}^*$, and D^*.[16]

3.2. Positively Charged Membrane. Without loss of generality, we assume that the membrane layer of a particle is positively charged. To ensure that the electrical potential of the system under consideration is not high, Q^* is assigned the value of 10;[34] for illustration, the corresponding electrical potential is then below 50 mV.[11] Figure 9 summarizes the simulated variations of the scaled electrophoretic mobility of the particle U^* under various conditions. Figure 9a−c reveals that the qualitative behavior of the relationship between U^* and (c/a) depends highly upon the levels of (b/a) and P, which is different from those shown in Figure 3a−c for the case where the membrane layer is uncharged. For example, as seen in Figure 9a,b, where (b/a) is small, if P is large (boundary effect is significant), then U^* decreases with increasing (c/a), which is similar to the results shown in Figure 3a−c. However, if P is small (boundary effect is insignificant), then U^* has a local maximum as (c/a) varies. In Figure 9c, where (b/a) is large (boundary effect is insignificant), U^* is seen to increase with increasing (c/a). The dependence of the relationship between U^* and (c/a) on the levels of (b/a) and P has not been reported in the literature and can be explained by the competition between the scaled net electrical driving force F_2^* ($= F_E^* + F_{D,2}^*$) and the hydrodynamic drag D^* as (c/a) varies. For the present case, the effective volume of the membrane layer increases with increasing (c/a), as do the amount of fixed charge, the associated scaled net electrical driving force F_2^*, and the hydrodynamic drag force. If the boundary effect is significant, then the rate of increase in D^* as (c/a) increases is faster than that in F_2^*, yielding a decrease in U^*, and that trend is reversed if the boundary effect is insignificant. As a result, if the boundary effect is moderate, then the behavior of U^* as (c/a) varies is dominated by both F_2^* and D^*, yielding the presence of a local maximum in U^* seen in Figure 9a,b. Figure 9 reveals that, regardless of

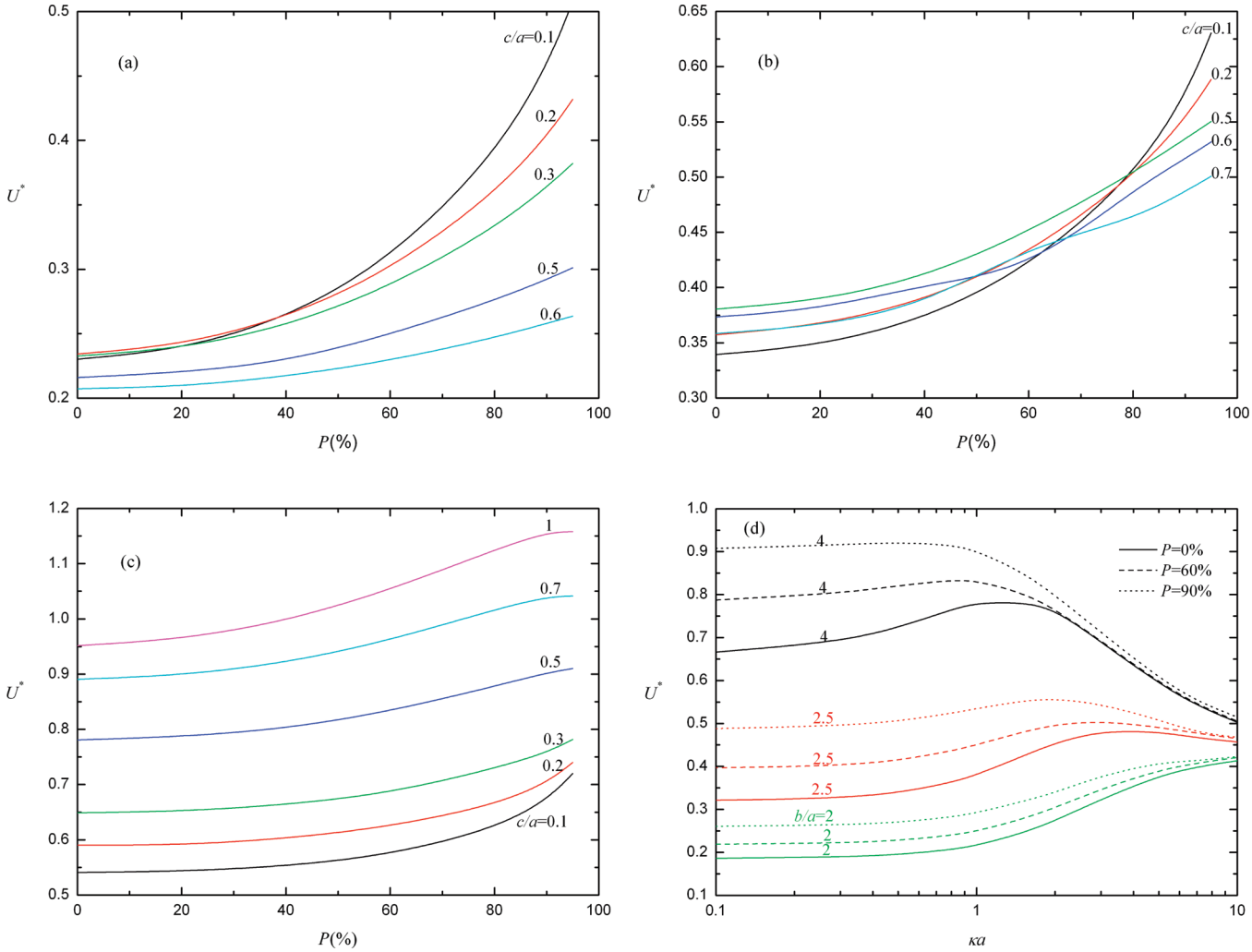

Figure 9. Variations of the scaled electrophoretic mobility U^* as a function of P for various combinations of (b/a) and (c/a) at $\kappa a = 1$ (a)−(c) and as a function of κa for various combinations of (b/a) and P at $c/a = 0.5$ (d), for the case where $Q^* = 10$, $\lambda a = 5$, and $d/a = 1$: (a) $b/a = 2$; (b) $b/a = 2.5$; (c) $b/a = 4$.

the levels of (c/a) and (b/a), U^* increases monotonically with increasing P; that is, the more the particle deviates from the axis of the pore, the larger its mobility. This is consistent with the result shown in Figure 3 and can be explained by the same reasoning. A comparison between Figure 3a−c and Figure 9a−c reveals that U^* is more sensitive to the variation of P in the case where the membrane layer is charged than that in the case where it is free of fixed charge. The general qualitative behavior of U^* as κa varies seen in Figure 9d is similar to that seen in Figure 3d and can be explained by the same reasoning. Figure 9d also indicates that, regardless of the levels of κa and P, U^* decreases with decreasing (b/a). This is because in the present case the rate of increase in D^* as (b/a) decreases is always faster than that in F_2^* ($= F_E^* + F_{D,2}^*$). It is interesting to note that the qualitative behavior of U^* as (b/a) varies, illustrated in Figure 9d, is different from that shown in Figure 3d. In the latter, that behavior depends upon the level of κa, which is unexpected.

Figure 10 illustrates the variations of the scaled electrophoretic mobility, U^*, and the associated scaled forces, F_E^*, $F_{D,2}^*$, and F_2^*, under various conditions. As seen in Figure 10a, similar to the case of an uncharged membrane, the qualitative behavior of U^* as κa varies depends upon the level of (c/a): if (c/a) is sufficiently small, U^* increases with increasing κa, and if (c/a) is large, then U^* has a local maximum as κa varies These behaviors can be explained by the results of F_E^*, $F_{D,2}^*$, and D^* illustrated in Figure 10b,c, and the reasoning similar to that in the discussion of Figure 5a can be applied. Figure 10a, where (b/a) takes a medium large value, also reveals that if P is sufficiently large (ca. 90%), then U^* decreases with increasing (c/a), but this trend becomes different if P is small (ca. 0%). In the latter, if κa is sufficiently large, U^* decreases with increasing (c/a), but if κa is small, then U^* shows a local maximum as (c/a) increases, which is not seen in Figure 5a, where the membrane layer is uncharged. The variation of the relationship between U^* and (c/a) as P varies, as seen in Figure 10a, has not been reported in the relevant literature,[33−36] where that relationship is described only by a result similar to that shown in Figure 9c ($b/a = 4$, boundary effect unimportant); that is, U^* increases monotonically with increasing (c/a). The results seen in Figure 10a arise mainly from the competition between F_2^* ($= F_E^* + F_{D,2}^*$) and D^* as P and (c/a) vary. As (c/a) increases, if P is sufficiently large (ca. 90%), then the rate of increase in D^* is always faster than that in F_2^*. This also occurs in the case where P is small and κa is sufficiently large. However, if both P and κa are sufficiently small, then the rate of increase in F_2^* is faster (slower) than that in D^* if (c/a) is small (large). As seen in Figure 10b,c, the behavior of F_E^* as κa varies depends upon the level of (c/a): if (c/a) is large, F_E^* decreases with increasing κa, and if (c/a) is small, then F_E^* has a local maximum as κa varies. These behaviors of F_E^* arise from the competition

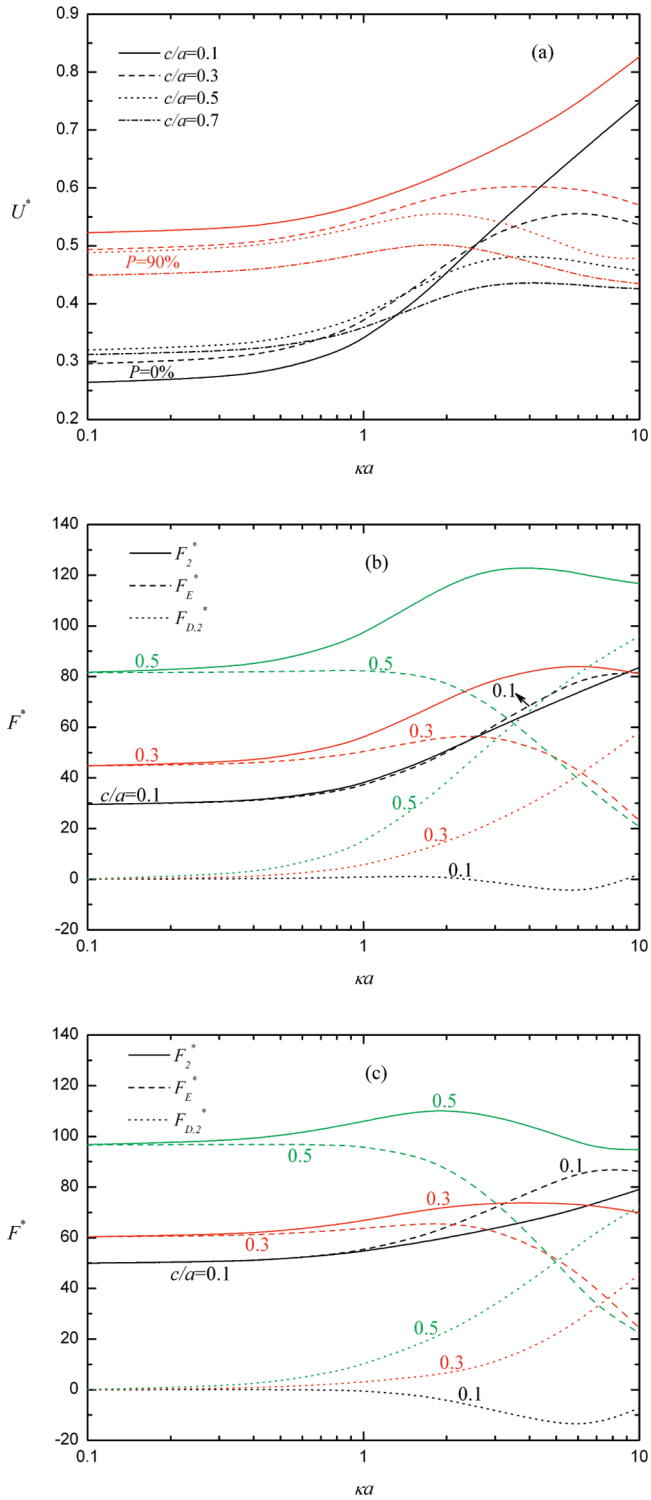

Figure 10. Variations of the scaled electrophoretic mobility U^* as a function of κa for various combinations of (c/a) and P at $b/a = 2.5$ and $d/a = 1$ for the case where $Q^* = 10$ and $\lambda a = 5$ (a), that of the scaled forces, F_E^*, $F_{D,2}^*$, and F_2^* for the case of Figure 10a at $P = 0\%$ (b), and that at $P = 90\%$ (c).

of two factors. First, because both the membrane layer and the rigid core of the particle are positively charged, $F_E^* > 0$. Therefore, the larger the κa (thinner double layer), the greater the amount of counterions confined in the interior of the membrane layer, which has the effect of reducing F_E^*, and this effect is enhanced, especially when the double layer is thinner than the membrane layer. Second, a thinner double layer also yields a greater electrical potential gradient on the surface of the rigid core of the particle, leading to a greater F_E^*. As seen in Figure 10b,c, the behavior of $F_{D,2}^*$ as κa varies depends on the level of (c/a): if (c/a) is large, then $F_{D,2}^*$ is always positive and increases with increasing κa. However, if (c/a) is sufficiently small, then $F_{D,2}^*$ is negative and has a negative local minimum as κa increases except when κa is sufficiently large. These behaviors, which arise from the competition between $F_{D,2(v)}^*$ and $F_{D,2(p)}^*$, are similar to those seen in Figures 4b,c and 5b, where the membrane layer is uncharged, and can be explained by the same reasoning. Note that the behavior of F_2^* in Figure 10b,c is similar to that of U^* in Figure 10a, implying that the behavior of U^* as κa varies is dominated by the scaled net electrical driving force F_2^* $(= F_E^* + F_{D,2}^*)$.

The variations of the scaled electrophoretic mobility of a particle U^* for various combinations of P, κa, (d/a), and (d/a) are presented in Figure 11. As seen in Figure 11a−c, regardless of the levels of κa and (d/a), U^* increases with increasing P, which is similar to the results shown in Figure 6a−c, where the membrane layer is uncharged. Figure 11d reveals that, regardless of the levels of (d/a) and P, U^* has a local maximum as κa varies, which is dissimilar to the result shown in Figure 6d at $d/a = 0.5$. Again, this can be explained by the behaviors of F_E^*, $F_{D,2}^*$, and D^*. Note that the relationship between U^* and (d/a) depends largely on the level of P. If P is small, then U^* decreases with increasing (d/a) if κa is small, and the reverse trend is observed if κa is large. On the other hand, if P is sufficiently large $(= 90\%)$, then U^* increases monotonically with increasing (d/a). These behaviors of U^* as (d/a) varies, shown in Figure 11d, are dissimilar to those for the case where the membrane layer is uncharged, shown in Figure 6d, and can be explained by the competition between F_2^* $(= F_E^* + F_{D,2}^*)$ and D^* as P and κa vary. In the present case, both the surface area of the rigid core of the particle and the effective volume of the membrane layer increase with increasing (d/a), as do F_2^* and D^*. Therefore, if P is sufficiently large, the behavior of U^* is dominated by the scaled net driving force associated with the electrical part, F_2^*, the rate of increase of which as (d/a) increases is always faster than that of D^*. However, if P is small, then the behavior of U^* is dominated by F_2^* if κa is large, and by D^* if κa is small, implying that the rate of increase in D^* as (d/a) increases is faster than that for F_2^* if κa is small, but that trend is reversed if κa is large. Note that the behavior of U^* as (d/a) varies in the present case (positively charged membrane layer) is similar to that in the corresponding case of a rigid cylinder[15,17,63] if P is small but becomes dissimilar if P is large.

The influence of the friction coefficient of the membrane layer of a particle, measured by λa, on its scaled electrophoretic mobility, U^*, is illustrated in Figure 12. The behavior of U^* in this figure is similar to that in Figure 8, where the membrane layer of a particle is uncharged and can be explained by the same reasoning. However, because the membrane layer is charged in the case of Figure 12, U^* has a local minimum as P varies, which occurs at a sufficiently large κa, only if λa is sufficiently large, as illustrated in Figure 12b. This is different from the results shown in Figure 8, where if κa is sufficiently large, then U^* has a local minimum as P varies for both a sufficiently small and a sufficiently large λa. The presence of a local minimum in U^* as P varies is also observed in the case of a rigid sphere in a circular cylindrical microchannel[10] and that of a rigid cylinder in a cylindrical pore.[16] This is because if λa is sufficiently large, then the present soft particle is close to a rigid particle.[33,37]

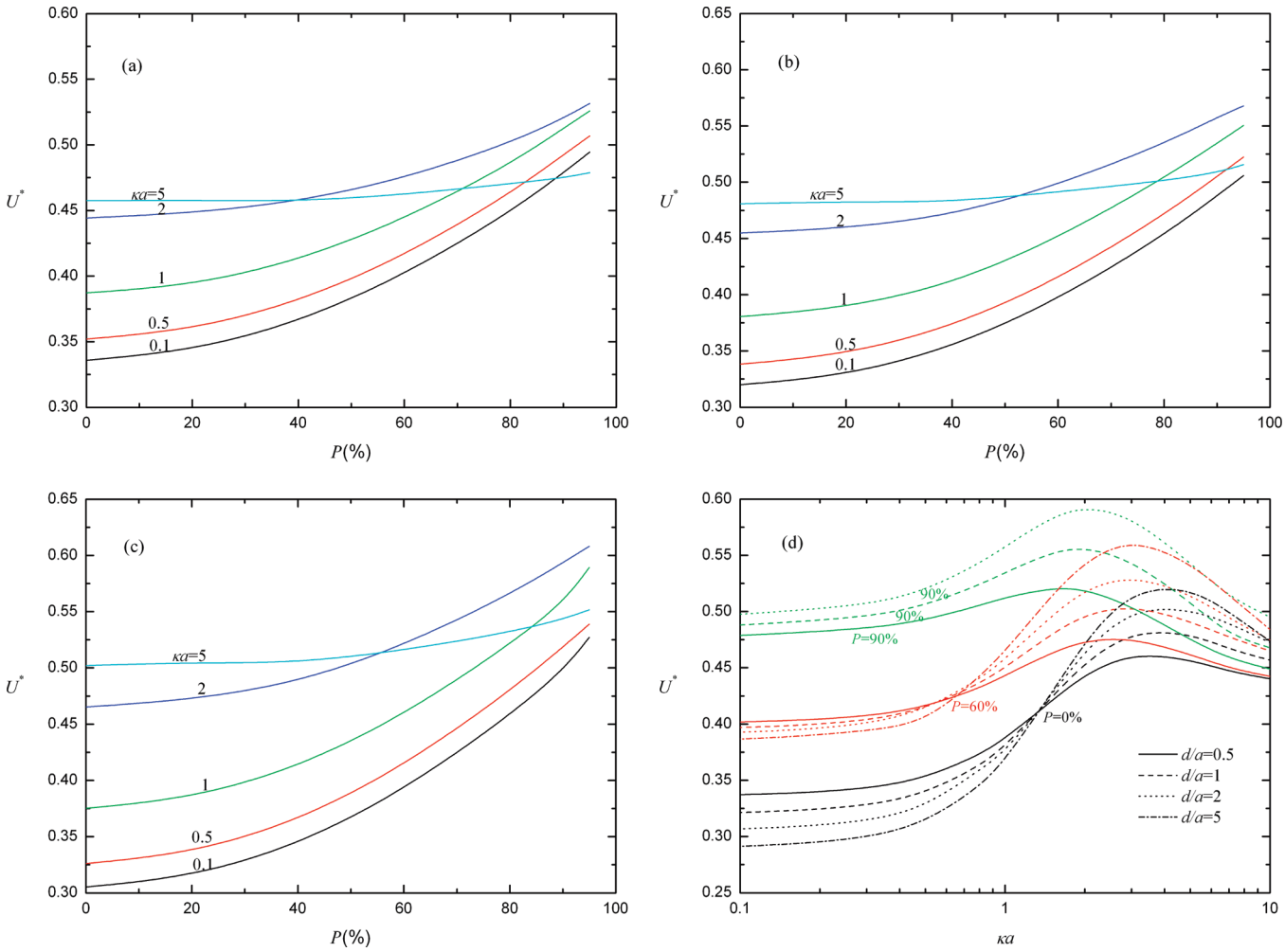

Figure 11. Variations of the scaled electrophoretic mobility U^* as a function of P for various combinations of (d/a) and κa at $b/a = 2.5$ and $c/a = 0.5$ (a)−(c) and as a function of κa for various combinations of (d/a) and P at $b/a = 2.5$ and $c/a = 0.5$ (d) for the case where $Q^* = 10$ and $\lambda a = 5$: (a) $d/a = 0.5$; (b) $d/a = 1$; (c) $d/a = 2$.

4. Conclusions

We extend the conventional electrophoresis analyses to a three-dimension case focusing on a soft particle, which is capable of simulating a wide class of particles in practice. The results obtained have potential applications such as probing the surface structure of biocolloids such as cells and microorganisms through microelectrophoresis. The electrophoretic behaviors of the soft particle under various conditions are examined through numerical simulations, and the results gathered can be summarized as follows. (i) If the membrane layer of a particle is uncharged, then the variation of its mobility as a function of double layer thickness depends largely on the pore size, and the thickness and the friction coefficient of the membrane layer, which is similar to the case where the membrane layer is positively charged. In addition, we show that the results for a rigid particle can be recovered from the present soft particle by reducing its membrane layer to become sufficiently thin. (ii) Similar to the case of a rigid particle, the larger the eccentricity of the soft particle, the larger its mobility is, in general. However, for the case where the membrane layer of a soft particle is uncharged, if the double layer is sufficiently thin, then the mobility of the particle may have a local minimum as its eccentricity varies, which occurs if the friction coefficient is either sufficiently small or sufficiently large. On the other hand, if the membrane layer is positively charged, this local minimum is present only if the friction coefficient is sufficiently large. (iii) If the membrane layer of a soft particle is uncharged, then its mobility decreases with increasing membrane layer thickness and/or friction coefficient and increases with increasing particle aspect ratio. In addition, if the double layer is sufficiently thick, then the mobility increases with increasing pore size. However, the opposite trend is observed if the double layer is sufficiently thin, which has not been found in similar electrophoresis problems. This implies that, depending upon the thickness of double layer, the boundary effect can either hinder or assist the movement of the soft particle. (iv) If the membrane layer of a soft particle is positively charged, then its mobility decreases with increasing friction coefficient, which is similar to the case of an uncharged membrane. However, depending upon the parameters chosen, the mobility may decrease, increase, or have a local maximum as the thickness of membrane layer varies, which has not been found in the literature. In addition, if the eccentricity of a soft particle is sufficiently large, then regardless of the thickness of double layer, the larger its aspect ratio, the larger its mobility. On the other hand, if the eccentricity is small, the mobility decreases with increasing aspect ratio if the double layer is thick, and that trend is reversed if the double layer is thin. If the membrane layer of a particle is positively charged, then its mobility increases monotonically with increasing pore

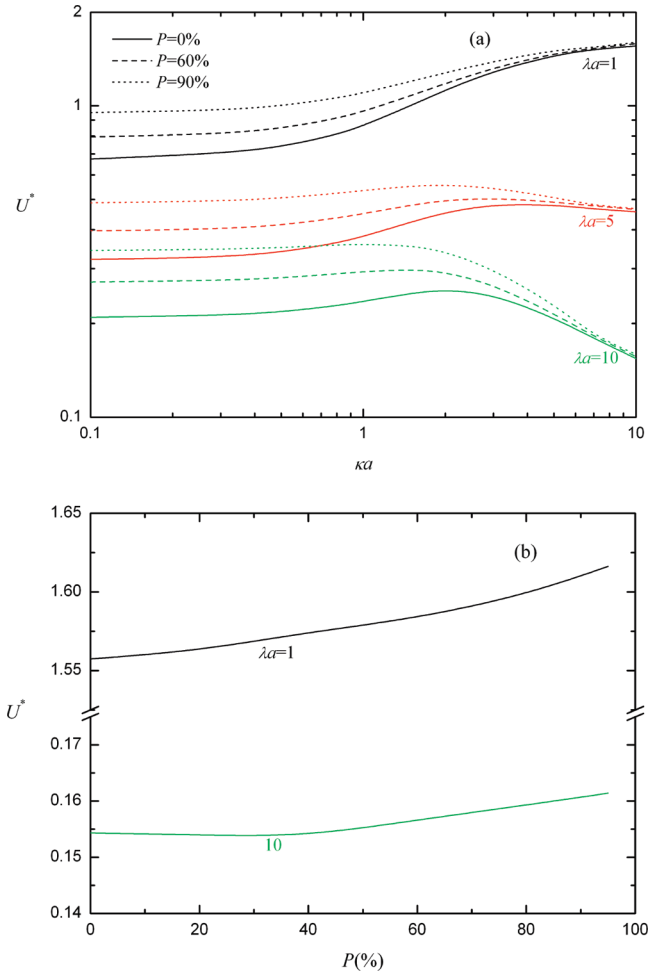

Figure 12. Variations of the scaled electrophoretic mobility U^* as a function of κa for various combinations of λa and P at $b/a = 2.5$, $c/a = 0.5$, $d/a = 1$, and $Q^* = 10$ (a) and as a function of P for two levels of λa at $\kappa a = 10$ for the case of Figure 12a (b).

size. These behaviors are dissimilar to those of the case where the membrane layer is uncharged.

Acknowledgment. This work is supported by the National Science Council of the Republic of China.

References and Notes

(1) Zydney, A. L. *J. Colloid Interface Sci.* **1995**, *169*, 476.
(2) Hsu, J. P.; Yeh, L. H.; Chen, Z. S. *J. Colloid Interface Sci.* **2007**, *310*, 281.
(3) Hsu, J. P.; Yeh, L. H. *Langmuir* **2007**, *23*, 8637.
(4) Hsu, J. P.; Chen, C. Y.; Yeh, L. H.; Tseng, S. *Colloids Surf. B* **2009**, *68*, 8.
(5) Keh, H. J.; Anderson, J. L. *J. Fluid Mech.* **1985**, *153*, 417.
(6) Shugai, A. A.; Carnie, S. L. *J. Colloid Interface Sci.* **1999**, *213*, 298.
(7) Hsu, J. P.; Yeh, L. H.; Yeh, S. J. *J. Phys. Chem. B* **2007**, *111*, 12351.
(8) Yariv, E.; Brenner, H. *Phys. Fluids* **2002**, *14*, 3354.
(9) Hsu, J. P.; Ku, M. H.; Kao, C. Y. *J. Colloid Interface Sci.* **2004**, *276*, 248.
(10) Ye, C.; Xuan, X.; Li, D. *Microfluid Nanofluid* **2005**, *1*, 234.
(11) Hsu, J. P.; Chen, Z. S. *Langmuir* **2007**, *23*, 6198.
(12) Qian, S. Z.; Joo, S. W.; Hou, W. S.; Zhao, X. *Langmuir* **2008**, *24*, 5332.
(13) Hsu, J. P.; Kao, C. Y. *J. Phys. Chem. B* **2002**, *106*, 10605.
(14) Liu, H.; Bau, H.; Hu, H. *Langmuir* **2004**, *20*, 2628.
(15) Hsu, J. P.; Ku, M. H. *J. Colloid Interface Sci.* **2005**, *283*, 592.
(16) Hsu, J. P.; Kuo, C. C. *J. Phys. Chem. B* **2006**, *110*, 17607.
(17) Yeh, L. H.; Hsu, J. P. *Microfluid Nanofluid* **2009**, *7*, 383.
(18) Tseng, S.; Cho, C. H.; Chen, Z. S.; Hsu, J. P. *Langmuir* **2008**, *24*, 2929.
(19) Hsu, J. P.; Kuo, C. C.; Ku, M. H. *Electrophoresis* **2006**, *27*, 3155.
(20) Hsu, J. P.; Yeh, L. H. *J. Phys. Chem. B* **2007**, *111*, 2579.
(21) Li, D.; Daghighi, Y. *J. Colloid Interface Sci.* **2010**, *342*, 638.
(22) Donath, E.; Pastuschenko, V. *Bioelectrochem. Bioenerg.* **1979**, *6*, 543.
(23) Wunderlich, R. W. *J. Colloid Interface Sci.* **1982**, *88*, 385.
(24) Levine, S.; Levine, M.; Sharp, K. A.; Brooks, D. E. *Biophys. J.* **1983**, *42*, 127.
(25) Sharp, K. A.; Brooks, D. E. *Biophys. J.* **1985**, *47*, 563.
(26) Ohshima, H.; Kondo, T. *Biophys. Chem.* **1991**, *39*, 191.
(27) Ohshima, H. *Adv. Colloid Interface Sci.* **1995**, *62*, 189.
(28) Zembala, M. *Adv. Colloid Interface Sci.* **2004**, *112*, 59.
(29) Duval, J. F. L.; Wilkinson, K. J.; van Leeuwen, H. P.; Buffle, J. *Environ. Sci. Technol.* **2005**, *39*, 6435.
(30) Lietor-Santos, J. J.; Fernandez-Nieves, A. *Adv. Colloid Interface Sci.* **2009**, *147*−*148*, 178.
(31) López-García, J. J.; Grosse, C.; Horno, J. *J. Colloid Interface Sci.* **2003**, *265*, 327.
(32) López-García, J. J.; Grosse, C.; Horno, J. *J. Colloid Interface Sci.* **2003**, *265*, 341.
(33) Lee, E.; Chou, K. T.; Hsu, J. P. *J. Colloid Interface Sci.* **2004**, *280*, 518.
(34) Lee, E.; Tong, Y. P.; Hsu, J. P. *Langmuir* **2004**, *20*, 9415.
(35) Hsu, J. P.; Chen, Z. S.; Tseng, S. *J. Phys. Chem. B* **2009**, *113*, 7701.
(36) Zhang, X.; Hsu, J. P.; Chen, Z. S.; Yeh, L. H.; Ku, M. H.; Tseng, S. *J. Phys. Chem. B* **2010**, *114*, 1621.
(37) Ohshima, H. *J. Colloid Interface Sci.* **1994**, *163*, 474.
(38) Ohshima, H. *J. Colloid Interface Sci.* **2000**, *228*, 190.
(39) Ohshima, H. *Electrophoresis* **2006**, *27*, 526.
(40) Ohshima, H. *Electrophoresis* **2002**, *23*, 1995.
(41) Ohshima, H. *J. Colloid Interface Sci.* **2002**, *252*, 119.
(42) Ohshima, H. *J. Colloid Interface Sci.* **2003**, *258*, 252.
(43) Saville, D. A. *J. Colloid Interface Sci.* **2000**, *222*, 137.
(44) Hill, R. J.; Saville, D. A.; Russel, W. B. *J. Colloid Interface Sci.* **2003**, *258*, 56.
(45) Cheng, W. L.; He, Y. Y.; Lee, E. *J. Colloid Interface Sci.* **2009**, *335*, 130.
(46) Corradini, D. *J. Chromatogr. B* **1997**, *699*, 221.
(47) Heller, C. *Electrophoresis* **2001**, *22*, 629.
(48) Henry, D. C. *Proc. R. Soc. London Ser. A* **1931**, *133*, 106.
(49) Hsu, J. P.; Yeh, L. H.; Ku, M. H. *J. Colloid Interface Sci.* **2007**, *305*, 324.
(50) Wei, Y. K.; Keh, H. J. *J. Colloid Interface Sci.* **2004**, *269*, 240.
(51) Hsu, J. P.; Yeh, L. H. *J. Chin. Inst. Chem. Eng.* **2006**, *37*, 601.
(52) Happel, J.; Brenner, H. *Low-Reynolds Number Hydrodynamics*; Nijhoff, M., Ed.; Kluwer: Boston, MA, 1983.
(53) O'Brien, R. W.; White, L. R. *J. Chem. Soc., Faraday Trans. 2* **1978**, *74*, 1607.
(54) Liu, J. K.; Lee, M. L. *Electrophoresis* **2006**, *27*, 3533.
(55) Aoyanagi, O.; Muramatsu, N.; Ohshima, H.; Kondo, T. *J. Colloid Interface Sci.* **1994**, *162*, 222.
(56) Kiers, P. J. M.; Bos, R.; van der Mei, H. C.; Busscher, H. J. *Microbiology* **2001**, *147*, 757.
(57) Rodriguez, V. V.; Busscher, H. J.; Norde, W.; van der Mei, H. C. *Electrophoresis* **2002**, *23*, 2007.
(58) Hoare, T.; Pelton, R. *Polymer* **2005**, *46*, 1139.
(59) Dague, E.; Duval, J.; Jorand, F.; Thomas, F.; Gaboriaud, F. *Biophys. J.* **2006**, *90*, 2612.
(60) Kuo, Y. C.; Lin, C. W. *Colloids Surf. B* **2009**, *71*, 45.
(61) Keh, H. J.; Chen, S. B. *J. Fluid Mech.* **1988**, *194*, 377.
(62) Dague, E.; Duval, J.; Jorand, F.; Thomas, F.; Gaboriaud, F. *Biophys. J.* **2006**, *90*, 2612.
(63) Sherwood, J. D. *J. Chem. Soc., Faraday Trans. 2* **1982**, *78*, 1091.

JP105572A